

Journal of Materials Chemistry C

Materials for optical, magnetic and electronic devices

Accepted Manuscript

This article can be cited before page numbers have been issued, to do this please use: A. K. Mohmand, X. Chen, S. Kumar, S. Yang, Y. Yu, W. Luo, Z. Jiang, M. Fung and L. Liao, *J. Mater. Chem. C*, 2020, DOI: 10.1039/D0TC01389G.



This is an Accepted Manuscript, which has been through the Royal Society of Chemistry peer review process and has been accepted for publication.

Accepted Manuscripts are published online shortly after acceptance, before technical editing, formatting and proof reading. Using this free service, authors can make their results available to the community, in citable form, before we publish the edited article. We will replace this Accepted Manuscript with the edited and formatted Advance Article as soon as it is available.

You can find more information about Accepted Manuscripts in the [Information for Authors](#).

Please note that technical editing may introduce minor changes to the text and/or graphics, which may alter content. The journal's standard [Terms & Conditions](#) and the [Ethical guidelines](#) still apply. In no event shall the Royal Society of Chemistry be held responsible for any errors or omissions in this Accepted Manuscript or any consequences arising from the use of any information it contains.

Spiro-Type Host Materials with Rigidified Skeleton for RGB Phosphorescent OLEDs

Aziz Khan, ‡ Xing Chen, ‡ Sarvendra Kumar, Sheng-Yi Yang, You-Jun Yu, Wei Luo, Zuo-Quan Jiang,* Man-Keung Fung,* and Liang-Sheng Liao

A. Khan, X. Chen, S. Kumar, S. Y. Yang, Y. J. You, W. Luo, Prof. M. K. Fung, Prof. Z. Q. Jiang, Prof. L. S. Liao

Institute of Functional Nano & Soft Materials (FUNSOM), Jiangsu Key Laboratory for Carbon-Based Functional Materials & Devices, Soochow University, 199 Ren'ai Road, Suzhou, 215123, Jiangsu, PR China

E-mail: zqjiang@suda.edu.cn; mkfung@suda.edu.cn

[‡] These authors contributed equally to this work.

Keywords: phosphorescent organic light-emitting diodes; RGB colors; high efficiency, spiro-type host; bipolar.

Abstract

The universal host material for red, green and blue is still a big challenge for fabricating efficient phosphorescent organic light-emitting diodes (PHOLEDs). Herein, two spiro host materials namely 3-(4,6-diphenyl-1,3,5-triazin-2-yl)-9',9'-dimethyl-9'H-spiro[fluorene-9,5'-quinolino[3,2,1-de]acridine] (**QAF-TRZ**) and 3'-(4,6-diphenyl-1,3,5-triazin-2-yl)-10-phenyl-10H-spiro[acridine-9,9'-fluorene] (**STF-TRZ**) are designed and synthesized. The designed strategy is more appropriate and rarely found among the reported spiro-based skeleton for organic light-emitting diodes (OLEDs). Both materials exhibited excellent electroluminescence performance. In particular, the RGB three-color PHOLEDs based on **QAF-TRZ**, **STF-TRZ** as hosts and **FIrpic**, **Ir(ppy)₂acac**, **Ir(MDQ)₂acac** as emitters are fabricated. The blue PHOLEDs

based on **QAF-TRZ** realize a maximum external quantum efficiency (EQE) of 19.4%, and remain 17.2% at 1000 cd/m². On the other hand, green PHOLEDs shows maximum EQEs of 21% and 19% for **QAF-TRZ** and **STF-TRZ**, respectively, and both devices exhibit low efficiency roll-off. Red devices obtain EQEs of 22.6 % and 19.4 % based on **QAF-TRZ** and **STF-TRZ**, respectively, in which the former has among the most efficient value. Consequently, these results confirm host materials incorporating spiro-motif having sufficiently high triplet energy are promising to obtain high-performances of RGB based PHOLEDs. The better device performance based on **QAF-TRZ** stems from its better hole transport capability, hence a superior charge recombination efficiency.

Introduction

Organic light-emitting diodes (OLEDs) have attracted widespread interest in both academia and industry, because of the fascinating applications in flat panel display and solid-state lighting.¹⁻⁵ Generally, in fluorescent OLEDs the non-radiative process limits the internal quantum efficiency (IQE) to 25% while the external quantum efficiency (EQE) hardly exceeds 5%.⁶ To resolve this issue, Forrest et al. represented phosphorescent organic light-emitting diodes (PHOLEDs) containing platinum (II) or iridium (III) complexes, which can successfully obtain 100% IQE via spin-orbit coupling, utilizing both singlet and triplet excitons.⁷⁻¹¹ Since then, many efforts have been made to improve device performance and stability. On the other hand, phosphorescent OLEDs doped with host material is also highly demanded to mitigate triplet-triplet annihilation and concentration quenching phenomena.^{12, 13} Host materials usually have two design strategies. Firstly, to prevent the reverse energy transfer from guest to host, the host materials must have a higher triplet energy level (E_T) than the guest. Secondly, to reduce the turn-on voltage and facilitate effective injection of hole and electron, suitable highest occupied molecular orbitals

(HOMOs) and the lowest unoccupied molecular orbitals (LUMOs) of the host to adjacent material layers are highly required.¹⁴⁻¹⁹

Compared with unipolar host,^{20, 21} bipolar host materials attracted more attention because of both the hole and electron transport elements can be found in a single molecule.²²⁻²⁷ In this regard, many groups strived to design bipolar host materials with good efficiency^{7, 22, 23, 28}. Among them, spiro-type²⁹⁻³⁶ bipolar hosts are of particular interest due to the following features: i) the 3-D configuration can enhance the thermal and morphological stabilities, ii) the functionalization of spiro-hosts is flexible, i.e. chemist has the room to modify not only the acceptor unit but also donor unit of the hemisphere, iii) this modification can balance hole/electron transport. In designing bipolar compounds in the most classic 9,9'-spirobifluorene, many electron-rich spiro backbones have been developed with appended electron acceptor (Scheme 1a).

Herein, two novel spiro-type bipolar host materials namely 3-(4,6-diphenyl-1,3,5-triazin-2-yl)-9',9'-dimethyl-9'H-spiro[fluorene-9,5'-quinolino[3,2,1-de]acridine] (**QAF-TRZ**) and 3'-(4,6-diphenyl-1,3,5-triazin-2-yl)-10-phenyl-10H-spiro[acridine-9,9'-fluorene] (**STF-TRZ**) containing 9,9-dimethyl-10-phenyl-9,10-dihydroacridine and triphenylamine donor linking with strong triazine acceptor through spiro bridge are prepared, respectively. In comparison, **QAF-TRZ** with new rigidified donor moiety has a prominent effect on photophysical, thermal properties and electroluminescence (EL) device performance. We systematically investigated both materials as universal hosts in blue/green/red PHOLEDs. As a result, the devices based on **QAF-TRZ** show superior performances and lower efficiency roll-off than **STF-TRZ**, indicating the potential of this new spiro-structure for PHOLED host.

Experimental Section

Compound 1 and 2' were purchased while compound 2 was synthesized according to proposed literature.^{37, 38}

3-bromo-9',9'-dimethyl-9'H-spiro[fluorene-9,5'-quinolino[3,2,1-de]acridine] (3)

The compound 2, (10-(2-bromophenyl)-9,9-dimethyl-9,10-dihydroacridine) (2.0 g, 5.6 mmol) was dissolved in THF (40 mL) under inert environment. The *n*-butyl lithium (1.6 M solution in hexane 2.2 mL, 5.5 mmol) was added slowly at -78 °C, and the reaction mixture was stirred for 1 hour at the same condition. Then THF solution (20 mL) of 3-bromo-9H-fluoren-9-one (1.1 g, 4.6 mmol) was added and further stirred for 2 hours at -78 °C. It is then stirred overnight at room temperature. After completion, the reaction mixture was quenched with water (5 mL). The THF was evaporated and the obtained viscous solid was extracted with dichloromethane (DCM) and washed with water (30 mL × 3). The organic portion was collected and purified through column about 1.8 g (72%) until white solid was obtained. which was used in the next reaction after purification. The intermediate 3-bromo-9-(2-(9,9-dimethylacridin-10(9H)-yl)phenyl)-9H-fluoren-9-ol was dissolved in acetic acid (30 mL) refluxed at 80 °C for 20 minutes. Then hydrochloric acid (8 mL) was added slowly to the reaction mixture. After 4 hours, white solid was appeared. It was filtered off and washed first with water and then petroleum ether (PE). Column chromatography was used for further purification: PE/ DCM (7/3, v/v) (1.6 g, 97%). ¹H NMR (400 MHz, CDCl₃) δ (ppm) 8.05 (d, *J* = 1.8 Hz, 1H), 7.88 (d, *J* = 7.6 Hz, 1H), 7.83 (d, *J* = 1.7 Hz, 1H), 7.72 (dd, *J* = 12.3, 4.3 Hz, 1H), 7.67 (d, *J* = 7.9 Hz, 1H), 7.60 (ddd, *J* = 8.1, 6.1, 1.5 Hz, 2H), 7.54 – 7.46 (m, 1H), 7.39 – 7.30 (m, 2H), 7.27 – 7.18 (m, 2H), 7.13 (d, *J* = 7.7 Hz, 1H), 7.07 (dd, *J* = 8.2, 1.8 Hz, 1H), 7.02 – 6.94 (m, 1H), 6.85 (td, *J* = 7.6, 3.0 Hz, 2H), 6.65 (ddd, *J* = 9.6, 7.9, 1.4 Hz, 1H), 6.45 (ddd, *J* = 9.0, 7.8, 1.2 Hz, 1H), 1.99 (s, 3H), 1.39 (s, 3H). ¹³C NMR (100 MHz, CDCl₃) δ (ppm) 154.60,

152.92, 150.51, 149.26, 144.90, 141.43, 139.18, 138.61, 136.98, 136.35, 135.57, 134.29, 131.71, 131.01, 129.11, 128.68, 128.42, 127.40, 126.79, 126.59, 125.41, 124.47, 124.03, 123.71, 123.61, 123.04, 122.51, 121.40, 120.37, 118.50, 116.91, 57.36, 36.93, 31.81, 23.02. MS (EI) m/z : 525.08 $[M^+]$.

3'-bromo-10-phenyl-10H-spiro[acridine-9,9'-fluorene] (3')

The intermediate 3' was synthesized according to the similar procedure as explained above for compound 3 except changing the corresponding reagents. Which was further purified from column chromatography with eluents: PE/ DCM (8/2, v/v) (1.3 g, 90%). ^1H NMR (400 MHz, CDCl_3) δ (ppm) 7.97 (d, $J = 1.7$ Hz, 1H), 7.83 – 7.71 (m, 3H), 7.62 (t, $J = 7.5$ Hz, 1H), 7.53 (d, $J = 8.4$ Hz, 2H), 7.50 – 7.39 (m, 3H), 7.32 (dd, $J = 18.3, 9.5$ Hz, 2H), 7.01 – 6.92 (m, 2H), 6.62 (t, $J = 7.5$ Hz, 2H), 6.42 (dd, $J = 16.2, 8.5$ Hz, 4H). ^{13}C NMR (100 MHz, CDCl_3) δ (ppm) 156.81, 155.39, 141.34, 140.96, 137.93, 131.16, 129.17, 128.56, 127.74, 127.38, 125.97, 124.01, 123.17, 121.69, 120.65, 120.17, 114.79, 56.66. MS (EI) m/z : 485.24 $[M^+]$.

9',9'-dimethyl-3-(4,4,5,5-tetramethyl-1,3,2-dioxaborolan-2-yl)-9'H-spiro[fluorene-9,5'-quinolino[3,2,1-de]acridine] (4)

A mixture of 3-bromo-9',9'-dimethyl-9'H-spiro[fluorene-9,5'-quinolino[3,2,1-de]acridine] (1.3 g, 2.4 mmol), 4,4,40,40,5,5,50,50-octamethyl-2,20-bi(1,3,2-dioxaborolane) (1.2 g, 4.9 mmol), 1,1'-bis(diphenylphosphino)ferrocene-palladium(II) ($\text{Pd}(\text{dppf})_2\text{Cl}_2$) 87.0 mg, 0.1 mmol), potassium acetate (1.1 g, 12.0 mmol), and anhydrous 1,4-dioxane (50 mL) was degassed and then refluxed under an inert atmosphere for 24 hours at 80 °C. The reaction mixture was washed three times with water (30 mL \times 3) after dilution with DCM. In order to remove water completely from the organic part, anhydrous MgSO_4 was added. The solvent of crude product was dried through rotary evaporator, which was purified using column chromatography to obtain a white powder with the

eluents: PE/ DCM (4/6, v/v) (1.1 g, 78%). ^1H NMR (400 MHz, CDCl_3) δ (ppm) 8.37 (s, 1H), 8.17 (s, 1H), 7.96 (dd, $J = 14.1, 7.5$ Hz, 1H), 7.80 – 7.69 (m, 1H), 7.68 – 7.54 (m, 2H), 7.53 – 7.42 (m, 2H), 7.38 – 7.29 (m, 2H), 7.18 (ddd, $J = 23.6, 14.6, 8.3$ Hz, 3H), 6.94 (t, $J = 7.5$ Hz, 1H), 6.82 (dd, $J = 9.2, 4.6$ Hz, 2H), 6.67 – 6.60 (m, 1H), 6.44 (t, $J = 7.2$ Hz, 1H), 1.98 (s, 3H), 1.47 (s, 6H), 1.39 (s, 3H), 1.32 (s, 6H). ^{13}C NMR (100 MHz, CDCl_3) δ (ppm) 153.73, 149.96, 139.28, 138.62, 136.99, 136.41, 135.24, 134.68, 134.19, 134.14, 129.23, 128.24, 128.06, 127.42, 127.13, 127.06, 126.90, 126.67, 126.46, 126.37, 124.39, 123.98, 123.85, 123.27, 123.02, 122.86, 122.11, 120.38, 120.34, 118.42, 118.38, 116.98, 116.92, 84.05, 83.72, 57.68, 36.92, 31.77, 31.66, 25.00, 24.83, 24.79, 23.02. MS (EI) m/z : 573.29 [M^+].

10-phenyl-3'-(4,4,5,5-tetramethyl-1,3,2-dioxaborolan-2-yl)-10H-spiro[acridine-9,9'-fluorene] (4')

The compound 4' was synthesized according to the similar procedure mention above for the compound 4 only by changing the corresponding reagents. In order to obtain pure product, it was passed through column chromatography with the eluents: PE/ DCM (4/6, v/v) (0.8 g, 66%). ^1H NMR (400 MHz, CDCl_3) δ (ppm) 8.30 (s, 1H), 7.88 (d, $J = 7.5$ Hz, 1H), 7.81 – 7.69 (m, 3H), 7.60 (t, $J = 8.0$ Hz, 1H), 7.53 (d, $J = 8.1$ Hz, 2H), 7.46 (dd, $J = 14.3, 7.5$ Hz, 2H), 7.39 (t, $J = 8.0$ Hz, 1H), 7.25 (d, $J = 7.4$ Hz, 1H), 6.97 – 6.89 (m, 2H), 6.57 (t, $J = 7.5$ Hz, 2H), 6.39 (dd, $J = 13.7, 7.3$ Hz, 4H), 1.42 (s, 12H). ^{13}C NMR (100 MHz, CDCl_3) δ (ppm) 159.53, 156.68, 141.17, 138.95, 135.10, 131.15, 128.40, 127.87, 127.58, 127.21, 126.33, 125.66, 125.35, 124.54, 120.54, 120.18, 114.63, 83.90, 56.97, 24.94. MS (EI) m/z : 533.35 [M^+].

3-(4,6-diphenyl-1,3,5-triazin-2-yl)-9',9'-dimethyl-9'H-spiro[fluorene-9,5'-quinolino[3,2,1-de]acridine] (QAF-TRZ)

The compounds 9',9'-dimethyl-3-(4,4,5,5-tetramethyl-1,3,2-dioxaborolan-2-yl)-9'H-spiro[fluorene-9,5'quinolino [3,2,1-de]acridine] (0.8 g, 1.5 mmol), 2-chloro-4,6-diphenyl-1,3,5 triazine (0.5 g, 1.8 mmol), tetrakis(triphenylphosphine)palladium(0) (50.0 mg, 0.05 mmol) and potassium carbonate (0.5 g, 3.7 mmol) were dissolved in 1,4-dioxane/ H₂O (40: 4), and refluxed for 24 hours at 85 °C. The mixture was diluted with DCM and washed thrice with distilled water (100 mL). The organic layer was dried and purified through column chromatography using PE/DCM (7/3, v/v) to obtain a pale white powder (0.8 g, 80%). ¹H NMR (600 MHz, CDCl₃) δ (ppm) 9.25 (s, 1H), 9.02 (s, 1H), 8.87 (dd, *J* = 14.1, 7.3 Hz, 2H), 8.73 (d, *J* = 7.1 Hz, 2H), 8.36 (d, *J* = 8.1 Hz, 1H), 8.14 (d, *J* = 7.6 Hz, 1H), 7.93 (d, *J* = 7.5 Hz, 1H), 7.79 (d, *J* = 8.0 Hz, 1H), 7.73 (d, *J* = 8.0 Hz, 1H), 7.70 – 7.48 (m, 8H), 7.36 (s, 1H), 7.31 (t, *J* = 7.2 Hz, 1H), 7.20 (t, *J* = 8.9 Hz, 1H), 7.15 (d, *J* = 7.6 Hz, 1H), 6.98 (t, *J* = 7.5 Hz, 1H), 6.83 (dd, *J* = 13.1, 7.2 Hz, 2H), 6.69 (dd, *J* = 14.3, 7.9 Hz, 1H), 6.49 (dd, *J* = 18.7, 7.8 Hz, 1H), 1.97 (s, 3H), 1.39 (s, 3H). ¹³C NMR (150 MHz, CDCl₃) δ (ppm) 171.73, 158.31, 155.01, 154.51, 150.38, 143.51, 142.24, 139.26, 138.69, 137.70, 137.03, 136.67, 136.16, 135.75, 134.32, 132.58, 131.96, 129.64, 129.42, 127.81, 127.04, 126.63, 124.51, 124.31, 123.39, 123.08, 122.39, 120.95, 118.56, 117.02, 57.79, 36.98, 31.84, 23.08. MALDI-TOF (*m/z*) calculated for C₄₉H₃₄N₄ [M⁺]: 678.27, found: 678.22. Anal. Calcd for C₄₉H₃₄N₄ C, 86.70; H, 5.05; N, 8.25 found C, 85.92; H, 4.97; N, 8.07.

3'-(4,6-diphenyl-1,3,5-triazin-2-yl)-10-phenyl-10H-spiro[acridine-9,9'-fluorene] (STF-TRZ).

A mixture of 10-phenyl-3'-(4,4,5,5-tetramethyl-1,3,2-dioxaborolan-2-yl)-10H-spiro[acridine-9,9'-fluorene] (0.7 g, 1.3 mmol), 2-chloro-4,6-diphenyl-1,3,5 triazine (0.4 g, 1.6 mmol), tetrakis (triphenylphosphine) palladium (0) (50.0 mg, 0.04 mmol) and potassium carbonate (0.4 g, 3.2

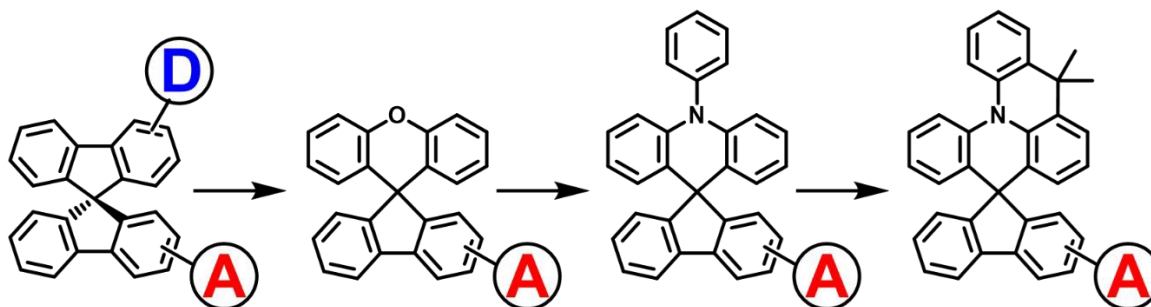
mmol) was dissolved in 1,4-dioxane/ H₂O (40: 4) refluxed over night at 85 °C. The crude organic layer was subjected to column chromatography for further purifications using PE/ DCM (7/3, v/v) (0.68 g, 81%). ¹H NMR (600 MHz, CDCl₃) δ (ppm) 9.15 (s, 1H), 8.81 (d, *J* = 6.9 Hz, 4H), 8.69 (d, *J* = 8.0 Hz, 1H), 8.05 (d, *J* = 7.5 Hz, 1H), 7.73 (t, *J* = 7.6 Hz, 2H), 7.68 – 7.56 (m, 8H), 7.54 (d, *J* = 7.8 Hz, 2H), 7.47 (dd, *J* = 17.7, 10.3 Hz, 2H), 7.33 (t, *J* = 7.4 Hz, 1H), 6.94 (t, *J* = 7.7 Hz, 2H), 6.58 (t, *J* = 7.4 Hz, 2H), 6.47 (d, *J* = 6.9 Hz, 2H), 6.39 (d, *J* = 8.4 Hz, 2H). ¹³C NMR (150 MHz, CDCl₃) δ (ppm) 171.83, 171.64, 160.63, 156.52, 141.28, 140.99, 139.87, 138.70, 136.25, 135.95, 132.51, 131.17, 131.08, 129.54, 128.97, 128.84, 128.65, 128.49, 127.77, 127.74, 127.39, 125.96, 125.87, 124.25, 120.63, 120.53, 120.40, 114.73, 57.03. MALDI-TOF (*m/z*) calculated for C₄₆H₃₀N₄ [M⁺]: 638.24, found: 638.18. Anal. Calcd for C₄₆H₃₀N₄ C, 86.49; H, 4.73; N, 8.77 found C, 85.58; H, 4.69; N, 8.39.

Results and Discussion

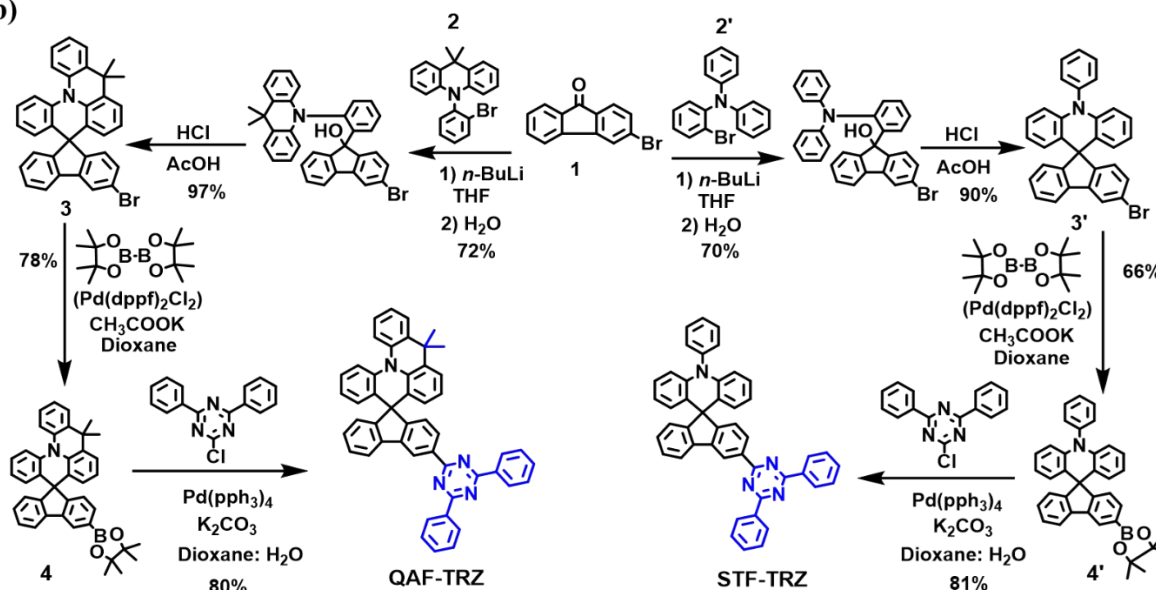
Synthesis and Characterization.

The synthetic routes for two compounds are depicted in Scheme 1b. The intermediate **3** and **3'** were synthesized through a three-step consecutive reaction under the same condition. Similarly, the intermediate **4** and **4'** were synthesized through the Miyaura borylation reaction.³⁹ Finally, the **QAF-TRZ** and **STF-TRZ** were successfully obtained in good yields through the Suzuki-Miyaura coupling reaction with 2-chloro-4,6-diphenyl-1,3,5 triazine and corresponding reagents **4** and **4'**. To make it highly pure, the products were further sublimated under vacuum after column chromatography before used in OLED devices. The chemical structures of **QAF-TRZ** and **STF-TRZ** were fully characterized through ¹HNMR, ¹³CNMR spectroscopy, mass spectrometry, and elemental analysis.

(a)



(b)



Scheme 1 (a) The derivatization way of donor/acceptor host materials in the spiro-skeleton. **(b)**

The synthetic routes for **QAF-TRZ** and **STF-TRZ**.

Thermal properties

The thermogravimetric analysis (TGA) and differential scanning calorimetry (DSC) under inert atmosphere were demonstrated in Fig. S1a and Fig. S1b for both compounds. The measured thermal properties and values are depicted in **Table 1**. The spiro annulated structure reveals high decomposition temperatures (T_d) with 5% weight loss observed at 430 and 424 °C, while the glass transition temperature (T_g) are 195 and 158 °C for **QAF-TRZ** and **STF-TRZ**, respectively.

Comparably, the **QAF-TRZ** has more favorable T_d and T_g over the **STF-TRZ** for OLED preparation in vacuum deposition due to the rigidification in spiro-skeleton.

Theoretical calculations

The theoretical calculations were performed to better understand the electronic properties of the two compounds by using density functional theory (DFT) and time-dependent DFT (TD-DFT). Ground-state geometries and excited state geometries were optimized at B3LYP/6-31G level.⁴⁰ The highest occupied molecular orbital (HOMO) and the lowest unoccupied molecular orbital (LUMO) of **QAF-TRZ** and **STF-TRZ** are mainly located at the donor and acceptor segment, respectively (Fig. 1a). The energy level of the HOMO and LUMO of **QAF-TRZ** and **STF-TRZ** are -5.04/-1.90 eV and -5.00/-1.74 eV, respectively (Fig. 1b); the fused strategy on donor leads to deeper HOMO and higher singlet/triplet energies as unveiled from the photophysical measurements (vide infra). Furthermore, the energy differences between S_1 and T_1 states for **QAF-TRZ** and **STF-TRZ** are almost same. Based on the electron-hole distribution analysis,⁴¹ 99.2% and 99.3% of the HOMO-to-LUMO transition contributed to the $S_0 \rightarrow S_1$ excitation for **QAF-TRZ** and **STF-TRZ**, respectively, while that contributed to the $S_0 \rightarrow T_1$ excitation was 98.0% and 96.7%, respectively, for the **QAF-TRZ** and **STF-TRZ**.

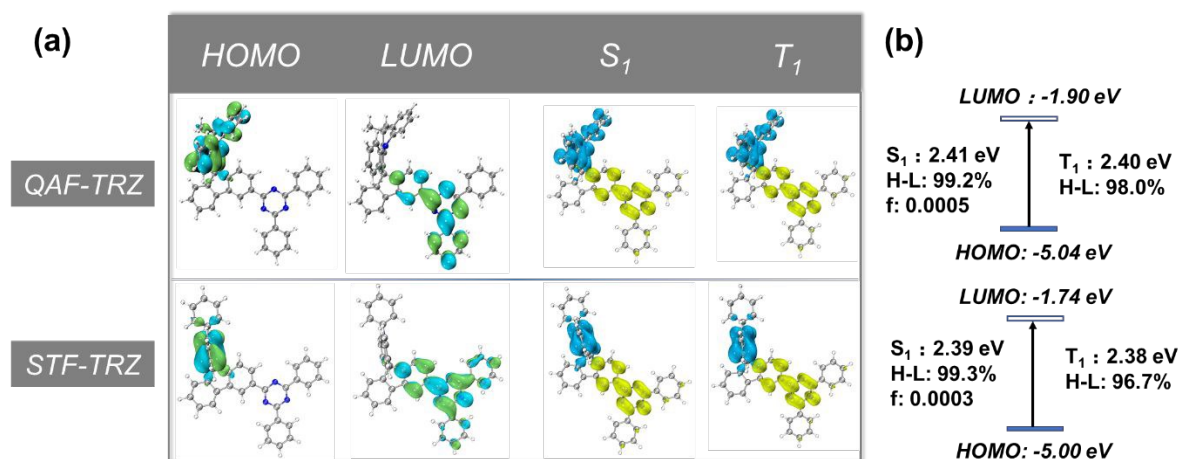


Fig. 1 (a) The distribution of HOMOs and LUMOs and the analysis for distribution of hole (blue), electron (yellow) for S₁ and T₁ and **(b)** energy level diagram of HOMOs, LUMOs, S₁ and T₁.

Photophysical properties.

The photophysical behavior of the **QAF-TRZ** and **STF-TRZ**, ultraviolet-visible (UV-vis) and fluorescence spectra were recorded in toluene at room temperature. Phosphorescence spectra were measured at frozen temperature (77 K) using the same solvent which are depicted in Fig. 2a and Fig. 2b respectively. **QAF-TRZ** and **STF-TRZ** show very similar absorption peak at 305 nm which is attributed to the π - π^* transitions. The HOMO-LUMO energy gaps were calculated from the UV absorption onset, and both are 3.44 eV. The fluorescence peaks as observed in the photoluminescence spectra (PL) for **QAF-TRZ** and **STF-TRZ** were 447 and 450 nm, respectively. Apart from that, the photophysical properties of **QAF-TRZ** and **STF-TRZ**, were also measured in neat film and their spectra are illustrated in Fig. S2. Notably, the absorption peak for **QAF-TRZ** and **STF-TRZ** is blue-shifted as compared of the solution results as well as the triplet-energy levels for **QAF-TRZ** and **STF-TRZ** are quite similar. Moreover, the triplet energies were calculated from the vibronic band of the phosphorescence spectra at 77 K are 2.88 eV for **QAF-**

TRZ, and 2.86 eV for **STF-TRZ**. Therefore, such triplet energies are high enough to prevent back energy transfer from emitters.

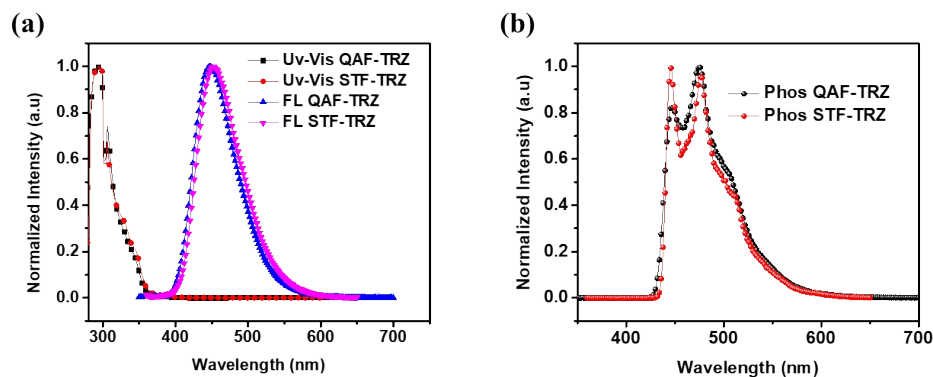


Fig 2. (a) Normalized UV-vis absorption and fluorescence emission spectra in toluene at room temperature. (b) Phosphorescence spectra in frozen toluene at 77 K for compounds **QAF-TRZ** and **STF-TRZ**.

Table 1. Summary of the physical properties of **QAF-TRZ** and **STF-TRZ**

Compounds	Abs^a (nm)	Fl^b (nm)	$Phos^c$ (nm)	E_g^d (eV)	E_T^e (eV)	HOMO/LUMO ^f (eV)	T_d/T_g^g (°C)
QAF-TRZ	305	447	447	3.44	2.88	-5.67/-2.23	430/195
STF-TRZ	305	450	446	3.44	2.86	-5.36/-1.91	424/158

^a Calculated from the UV-vis absorption measured in toluene. ^b Determined from the room temperature fluorescence in toluene. ^c Calculated from the 77 K phosphorescence in toluene. ^d Calculated from the UV-vis absorption in toluene. ^e Calculated from the phosphorescence in toluene. ^f HOMO is calculated from the oxidation potential with respect to reference ferrocene; LUMO is calculated from the energy gap plus HOMO. ^g T_d : Decomposition temperature, T_g : glass transition temperature.

Electrochemical Properties

To investigate the electrochemical behavior of the two host materials, **QAF-TRZ** and **STF-TRZ**, cyclic voltammetry analysis was performed in anhydrous DCM using the ferrocene as the internal standard and the parameters are summarized in Table 1. The oxidation potential values for the

compounds **QAF-TRZ** and **STF-TRZ** are +1.37 V and +1.05 V, respectively. The obtained results indicate that **QAF-TRZ** is constructed with a rigid donor structure as compared to **STF-TRZ**. The HOMO energy levels were estimated from the onset of the oxidation potential curves, to be -5.67/-5.36 eV, respectively, while the LUMO energy levels were calculated from E_g (onset of UV-vis spectra) and HOMO values, which were -2.23/-1.91 eV for **QAF-TRZ** and **STF-TRZ**, respectively (Fig. S3).

Electroluminescence (EL) Properties.

To further evaluate the EL properties of these two host materials, firstly we fabricated blue PHOLED devices based on **FIrpic**. As shown in Fig. 3a, the blue device structure is ITO/1,4,5,8,9,11-hexaazatriphenylene-hexacarbonitrile (HAT-CN) (10 nm)/ 1,1-bis[4-[N, N-di(p-tolyl)amino]phenyl]cyclohexane (TAPC) (40 nm)/ tris(4-(9H-carbazol-9-yl)phenyl)amine (TCTA) (10 nm)/ **QAF-TRZ** or **STF-TRZ**: **FIrpic** 15 wt% (20 nm)/ 3,3'-(5'-(3-(pyridin-3-yl)phenyl)-[1,1':3',1''-terphenyl]-3,3''-diyl)dipyridine (TmPyPB) (45 nm)/ (8-quinolinolato lithium) Liq (2 nm)/ Al (100 nm) (**B1** for **QAF-TRZ** and **B2** for **STF-TRZ**). The energy level diagrams of all the blue, green and red devices fabricated in the present studies are displayed in Fig. 3b. ITO acts as the anode while Al as the cathode. HAT-CN and Liq are the hole and electron-injection layers, respectively. TAPC is employed as the hole transport layer because of its remarkable hole mobility and TCTA plays the role as the electron blocking layer. Furthermore, TmPyPB is chosen as the electron transport layer for better energy level alignment. The chemical structures of these commercial materials are shown in Fig. S4. We all know that the E_T of PHOLED host is higher than that of the emitters for effective exciton confinement, better energy transfers from the host to the guest and reducing the non-radiative transition. In this work, the E_T of **QAF-TRZ** and **STF-TRZ** are 2.88 and 2.86 eV, respectively, which tells that all are appropriate as the host for **FIrpic**

($E_T = 2.62$ eV). We first fabricated the blue devices by varying the concentration of FIrpic from 10 to 20% (Table S1), and the optimized concentration was 15%. The current density-voltage-luminance (J - V - L) characteristics for both **B1** and **B2** are shown in Fig. S5a and their device performance is summarized in Table 2. Device **B1** exhibits a maximum EQE, current efficiency (CE), and power efficiency (PE) of 19.4%, 45 cd/A and 47.8 lm/W, respectively. The EQE can be maintained as 17.2% at 1000 cd/m². However, device **B2** shows a maximum EQE, CE, and PE of 12.7%, 30.8 cd/A and 27.5 lm/W, which reveals an apparently lower device performance as compared with **B1** (Fig. 3c). Conventional hosts such as 1,3-Bis(N-carbazolyl)benzene (mCP) and 2,6-bis(3-(carbazol-9-yl)phenyl)pyridine (26DCzppy) were also used for comparison. The device results are summarized in Table S2. Among them, QAF-TRZ shows the best device performance, making it a good candidate as a host material for PhOLED.

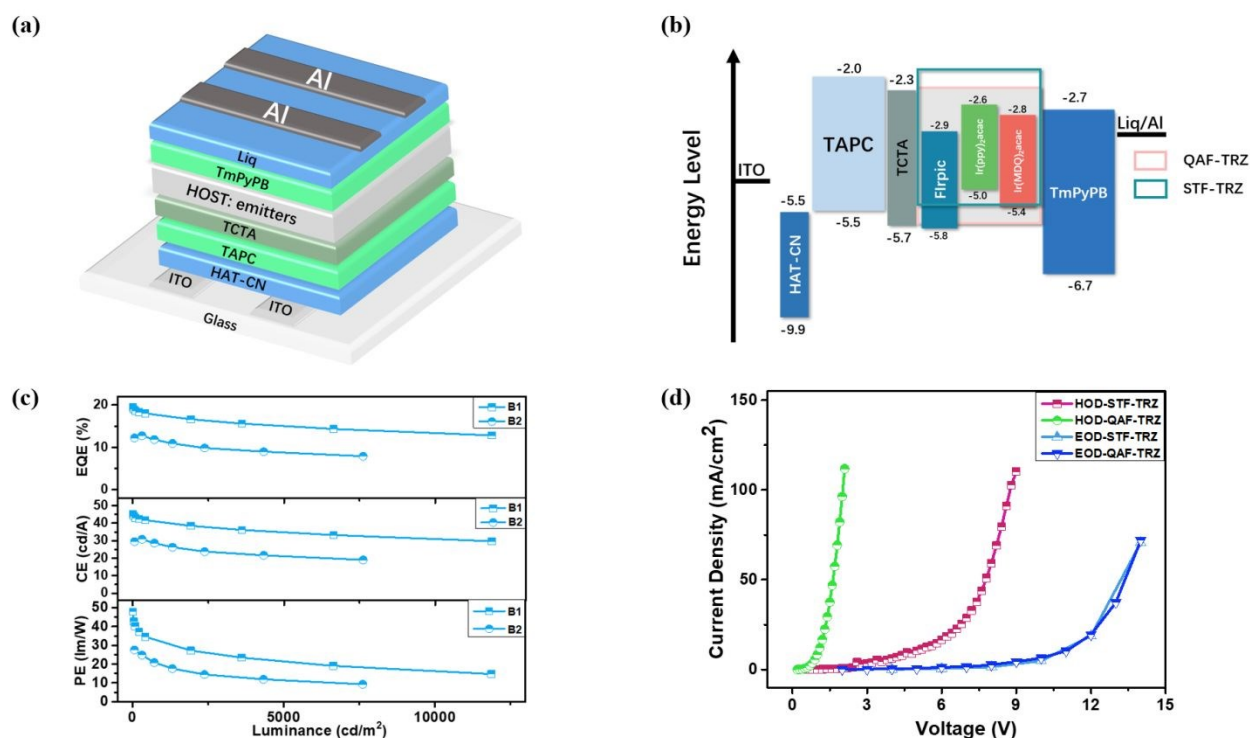


Fig. 3 (a) Device structure, (b) energy level diagrams of devices, (c) blue PHOLED performance

and **(d)** hole-only and electron-only devices based on **QAF-TRZ** and **STF-TRZ**.

Table 2 Electroluminescence characteristics of the devices

Device	V ^a (V)	CE ^b (cd/A)	PE ^b (lm/W)	EQE ^c (%)	CIE ^d (x,y)
B1	3.4	45.0	47.8	19.4/18.3/17.2	(0.16,0.35)
B2	3.5	30.8	27.5	12.7/12.3/11.3	(0.17,0.37)
G1	2.8	80.0	91.0	21.0/20.4/20.0	(0.34,0.63)
G2	2.9	72.0	76.0	19.0/18.9/18.8	(0.34,0.61)
R1	3.8	26.5	24.1	22.6/21.8/17.1	(0.63,0.36)
R2	3.8	29.0	25.3	19.4/19.0/15.5	(0.62,0.37)

^aDriving voltage at 100 cd/m²; ^bMaximum value of current efficiency and power efficiency; ^cEQEs of maximum value, 100 cd/m² and 1000 cd/m²; ^dCIE (Commission International de l'Eclairge); Measured at a driving current density at 5 mA/cm²

To further investigate the difference in the blue PHOLED performance under the same device structure, we fabricated electron- and hole-only devices (**EOD** and **HOD**) to estimate their charge mobilities. The device structures are as follows: ITO/ TmPyPB (20 nm)/ **QAF-TRZ** or **STF-TRZ** (100 nm)/ TmPyPB (20 nm)/ Liq (2 nm)/ Al (100 nm) (as **EOD**) and ITO/ MoO₃ (10 nm)/ **QAF-TRZ** or **STF-TRZ** (100 nm)/ MoO₃ (10 nm)/ Al (100 nm) (as **HOD**). As shown in Fig. 3d, the *J-V* curves of **QAF-TRZ** and **STF-TRZ** almost overlap under the same driving voltages in the **EOD** device, indicating that two host materials have the similar electron mobility. On the contrary, **QAF-TRZ** shows a higher current density than **STF-TRZ** at a low driving voltage in the **HOD**. Therefore, the better hole mobility of **QAF-TRZ** may more favor the hole-electron combination for forming exciton in the device **B1**.

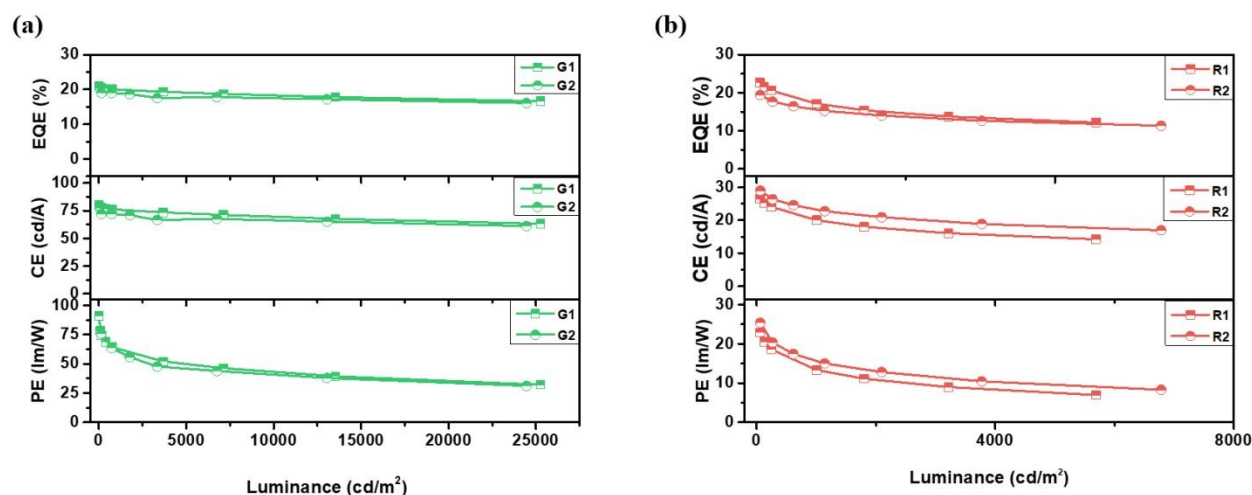


Fig. 4 (a) Green and (b) red PHOLEDs device performance for QAF-TRZ and STF-TRZ

Furthermore, green and red PHOLEDs were also fabricated with device structures of ITO/ HAT-CN (10 nm)/ TAPC (40 nm)/ TCTA (10 nm)/ **QAF-TRZ** or **STF-TRZ**: **Ir(ppy)₂acac** 10 wt% (20 nm)/ TmPyPB (45 nm)/ Liq (2 nm)/ Al (100 nm) and ITO/ HAT-CN (10 nm)/ TAPC (40 nm)/ TCTA (10 nm)/ **QAF-TRZ** or **STF-TRZ**: **Ir(MDQ)₂acac** 6 wt% (20 nm)/ TmPyPB (50 nm)/ Liq (2 nm)/ Al (100 nm) (**G1**, **R1** for **QAF-TRZ** and **G2**, **R2** for **STF-TRZ**). The E_T s of green (**Ir(ppy)₂acac**) and red (**Ir(MDQ)₂acac**) emitters are 2.4 eV and 2.0 eV, respectively, which are much lower than those of the hosts, and therefore can realize effective energy transfer. The device performance is shown in Fig. 4 and also summarized in Table 2. It can be seen that the maximum EQE, CE, and PE of **R1** and **R2** are 22.6%, 26.5 cd/A, 24.1 lm/W and 19.4%, 29.0 cd/A, 25.3 lm/W, respectively. The EQE of **R1** based on the **QAF-TRZ** is among the highest value in red PHOLEDs. Also, the EQE can be kept as high as 17.1% at 1000 cd/m². Moreover, the green devices (**G1** and **G2**) based on our two host materials exhibit maximum EQE, CE, PE, of 21.0%, 80 cd/A, 91 lm/W and 19%, 72 cd/A, 76 lm/W, respectively. Notably, **G1** and **G2** have quite similar performance and low-efficiency roll-off. At a luminance of 1000 cd/m², the EQE of devices

G1 and **G2** remain 20% and 18.8%, and merely decrease by 4% and 1% from their maximum values, respectively. This low roll-off property is mainly attributed to the well-balanced charge injection and better recombination arisen from the high E_T of the hosts. The J - V - L characteristics of green and red devices are exhibited in Fig. S5b and Fig. S5c, respectively. In addition, both hosts almost lead to identical RGB EL emissions (Fig. S5d), i.e. 472 nm for **B1** and **B2**, 524 nm for **G1** and **G2**, and 612 nm for **R1** and **R2**. Thus, there is no any other emission peak in the EL spectra, substantiating an efficient energy transfer from the hosts to the emitters.

Conclusion

We have designed and synthesized two host materials, **QAF-TRZ** and **STF-TRZ**, for red, green and blue PhOLEDs. Both materials have an excellent thermal property with a high T_d of over 420 °C. The EQE of the blue PhOLED reached nearly 20% when using **QAF-TRZ** as the host. The maximum EQEs for the green PhOLEDs **QAF-TRZ** and **STF-TRZ** as the hosts were 21% and 19%, respectively. Both the green PhOLEDs exhibited a low-efficiency roll-off, in which the EQEs merely decreased by 4% and 1%, respectively, from their maximum values when the devices were driven to a luminance of 1000 cd/m². Moreover, the red PhOLEDs exhibited maximum EQEs of 22.6% and 19.4% with using **QAF-TRZ** and **STF-TRZ** as the hosts, respectively, in which the former has the best EQE among all the red PhOLEDs. The superior device performance is attributed to the new rigidified donor moiety with the spiro motif incorporating triazine (at para position) type acceptors. Device based on **QAF-TRZ** even have higher efficiencies because it has a higher hole mobility with better charge recombination. We believe our simple spiro-skeleton strategy can facilitate the development of efficient and stable hosts for RGB based PhOLEDs.

Acknowledgments

We acknowledge financial support from the National Key R&D Program of China (No. 2016YFB0400700), the National Natural Science Foundation of China (Nos. 51773141, 51873139 and 21572152) and the Natural Science Foundation of Jiangsu Province of China (BK20181442). This project is also funded by Collaborative Innovation Center of Suzhou Nano Science & Technology, the Priority Academic Program Development of Jiangsu Higher Education Institutions (PAPD), the 111 Project of The State Administration of Foreign Experts Affairs of China. We greatly thank Yang-Kun Qu for analyzing the molecular simulations.

References

1. X.-D. Zhu, Y.-L. Zhang, Y. Yuan, Q. Zheng, Y.-J. Yu, Y. Li, Z.-Q. Jiang and L.-S. Liao, *J. Mater. Chem. C*, 2019, **7**, 6714-6720.
2. S. J. Kim, Y. J. Kim, Y. H. Son, J. A. Hur, H. A. Um, J. Shin, T. W. Lee, M. J. Cho, J. K. Kim and S. Joo, *Chem. Commun.*, 2013, **49**, 6788-6790.
3. M. Hu, Y. Liu, Y. Chen, W. Song, L. Gao, H. Mu, J. Huang and J. Su, *RSC Adv.*, 2017, **7**, 7287-7292.
4. C. W. Tang and S. A. VanSlyke, *Appl. Phys. Lett.*, 1987, **51**, 913-915.
5. W. Jiang, L. Duan, J. Qiao, D. Zhang, G. Dong, L. Wang and Y. Qiu, *J. Mater. Chem.*, 2010, **20**, 6131-6137.
6. L.-S. Cui, S.-B. Ruan, F. Bencheikh, R. Nagata, L. Zhang, K. Inada, H. Nakanotani, L.-S. Liao and C. Adachi, *Nat. Commun.*, 2017, **8**, 1-8.
7. R. K. Konidena, K. H. Lee and J. Y. Lee, *Chem. Asian J.*, 2019, **14**, 313-321.
8. M. Romain, S. Thiery, A. Shirinskaya, C. Declairieux, D. Tondelier, B. Geffroy, O. Jeannin, J. Rault-Berthelot, R. Métivier and C. Poriol, *Angew. Chem. Int. Ed.*, 2015, **54**, 1176-1180.

9. Y. Zhang, J. Lee and S. R. Forrest, *Nat. Commun.*, 2014, **5**, 1-7.
10. C. Adachi, M. A. Baldo, S. R. Forrest and M. E. Thompson, *Appl. Phys. Lett.*, 2000, **77**, 904-906.
11. S. Ye, Y. Liu, K. Lu, W. Wu, C. Du, Y. Liu, H. Liu, T. Wu and G. Yu, *Adv. Funct. Mater.*, 2010, **20**, 3125-3135.
12. P. Wu, W. Song, Z. Xia, Y. Chen, G. Tian, J. Huang and J. Su, *Dyes Pigm.*, 2019, **162**, 153-159.
13. Q. Dong, F. Tai, H. Lian, Z. Chen, M. Hu, J. Huang and W.-Y. Wong, *Dyes Pigm.*, 2017, **143**, 470-478.
14. M. A. Baldo, D. O'brien, M. Thompson and S. Forrest, *Phys. Rev. B*, 1999, **60**, 14422.
15. M. A. Baldo, D. O'brien, Y. You, A. Shoustikov, S. Sibley, M. Thompson and S. R. Forrest, *Nature*, 1998, **395**, 151-154.
16. M. H. Tsai, H. W. Lin, H. C. Su, T. H. Ke, C. C. Wu, F. C. Fang, Y. L. Liao, K. T. Wong and C. I. Wu, *Adv. Mater.*, 2006, **18**, 1216-1220.
17. D. Zhang, C. Zhao, Y. Zhang, X. Song, P. Wei, M. Cai and L. Duan, *ACS Appl. Mater. Interfaces*, 2017, **9**, 4769-4777.
18. S.-R. Park, S.-M. Kim, J.-H. Kang, J.-H. Lee and M. C. Suh, *Dyes Pigm.*, 2017, **141**, 217-224.
19. X. Zhan, Z. Wu, Y. Lin, Y. Xie, Q. Peng, Q. Li, D. Ma and Z. Li, *Chem. Sci.*, 2016, **7**, 4355-4363.
20. Z. Hu, W. Fu, L. Yan, J. Miao, H. Yu, Y. He, O. Goto, H. Meng, H. Chen and W. Huang, *Chem. Sci.*, 2016, **7**, 5007-5012.

21. V. Govindan, K.-C. Yang, Y.-S. Fu and C.-G. Wu, *New J. Org. Chem.*, 2018, **42**, 7332-7339.
22. A. Chaskar, H. F. Chen and K. T. Wong, *Adv. Mater.*, 2011, **23**, 3876-3895.
23. K. S. Yook and J. Y. Lee, *Adv. Mater.*, 2012, **24**, 3169-3190.
24. K. S. Yook and J. Y. Lee, *Chem. Rec.*, 2016, **16**, 159-172.
25. T. Chatterjee, W.-Y. Hung, W.-F. Tang, H.-F. Chen and K.-T. Wong, *Org. Electron.*, 2017, **50**, 204-212.
26. S. Kumar, D. Li, Y.-K. Wang, Y. Yuan, A. Khan, Z.-Q. Jiang and L.-S. Liao, *Synth. Met.*, 2019, **254**, 42-48.
27. D. Thirion, J. Rault-Berthelot, L. Vignau and C. Poriol, *Org. Lett.*, 2011, **13**, 4418-4421.
28. Y. Tao, C. Yang and J. Qin, *Chem. Soc. Rev.*, 2011, **40**, 2943-2970.
29. M. Romain, D. Tondelier, J. C. Vanel, B. Geffroy, O. Jeannin, J. Rault-Berthelot, R. Métivier and C. Poriol, *Angew. Chem. Int. Ed.*, 2013, **52**, 14147-14151.
30. C. Poriol, N. Cocherel, J. Rault-Berthelot, L. Vignau and O. Jeannin, *Chem. Eur. J.*, 2011, **17**, 12631-12645.
31. C. Poriol, J. Rault-Berthelot, F. Barriere and A. M. Slawin, *Org. Lett.*, 2008, **10**, 373-376.
32. L. Sicard, C. Quinton, J. D. Peltier, D. Tondelier, B. Geffroy, U. Biapo, R. Métivier, O. Jeannin, J. Rault-Berthelot and C. Poriol, *Chem. Eur. J.*, 2017, **23**, 7719-7727.
33. J. D. Peltier, B. Heinrich, B. Donnio, O. Jeannin, J. Rault-Berthelot and C. Poriol, *Chem. Eur. J.*, 2017, **23**, 17290-17303.
34. I. Bulut, P. Chávez, S. Fall, S. Méry, B. Heinrich, J. Rault-Berthelot, C. Poriol, P. Lévêque and N. Leclerc, *RSC Adv.*, 2016, **6**, 25952-25959.

35. C. Poriel, J. J. Liang, J. Rault-Berthelot, F. Barrière, N. Cocherel, A. M. Slawin, D. Horhant, M. Virboul, G. Alcaraz and N. Audebrand, *Chem. Eur. J.*, 2007, **13**, 10055-10069.
36. F. Moreau, N. Audebrand, C. Poriel, V. Moizan-Baslé and J. Ouvry, *J. Mater. Chem.*, 2011, **21**, 18715-18722.
37. Y. K. Wang, Q. Sun, S. F. Wu, Y. Yuan, Q. Li, Z. Q. Jiang, M. K. Fung and L. S. Liao, *Adv. Funct. Mater.*, 2016, **26**, 7929-7936.
38. A. Khan, Y.-K. Wang, C.-C. Huang, S. Kumar, M.-K. Fung, Z.-Q. Jiang and L.-S. Liao, *Org. Electron.*, 2019, 105520.
39. T. Liu, H. Sun, C. Fan, D. Ma, C. Zhong and C. Yang, *Org. Electron.*, 2014, **15**, 3568-3576.
40. P. J. Stephens, F. J. Devlin, C. F. Chabalowski and M. J. Frish, *J. Phys. Chem.*, 1994, **98**, 11623-11627.
41. L. Tian and F. W. Chen, *J. Comput. Chem.*, 2012, **33**, 580-592.

